SvedbergOpen
DISSEMINATION OF KNOWLEDGE
International Journal of Artificial Intelligence and Machine Learning
Publisher's Home Page: https://www.svedbergopen.com/
Research Paper
Open Access

Design And Analysis Of An Integrated Dq-Frame Control Strategy For Three-Phase Grid-Connected PV Systems

Vishal G. Jotangiya[1*], Riaz K. Israni[2], Chiragkumar Parekh[3] and Parin H. Chauhan[4]

[1] Research Scholar, Department of Electrical Engineering, RK University, Rajkot-360020, Gujarat, India; E-mail: vgjotangiya@gmail.com
[2] Associate Professor, Department of Electrical Engineering, RK University, Rajkot-360020, Gujarat, India; E-mail: riaz.israni@rku.ac.in
[3] Professor, Department of Electrical Engineering, RK University, Rajkot-360020, Gujarat, India; E-mail: chirag.parekh@rku.ac.in
[4] Assistant Professor, Electrical Engineering Department, Lukhdhirji Engineering College, Morbi-363642, Gujarat, India; E-mail: chauhanparin@gmail.com
* Correspondence: vgjotangiya@gmail.com

Abstract: To enhance the grid integration of single-stage, three-phase photovoltaic (PV) systems, this paper proposes a robust dq-frame control scheme for independent and precise regulation of active and reactive power. The proposed control algorithm generates reference currents directly from the desired active power (P) and reactive power (Q) power commands, which are then tracked by a dedicated current control loop to ensure fast dynamic response and improved stability under grid disturbances. When local loads are connected at the point of common coupling (PCC), the control strategy enables effective sharing of active and reactive power between the PV inverter and the utility grid according to predefined references, thereby maintaining voltage stability and reliable power delivery. In addition to basic power injection, the framework supports flexible power factor control for grid support and reactive power compensation. The paper presents the formulation of reference current generation, controller design, and grid synchronization methodology. MATLAB/Simulink simulation results validate the effectiveness of the proposed approach in terms of fast response, accurate power tracking, and enhanced operational reliability.

Keywords: Current Mode Control, DC-link voltage control, Grid Integration, Renewable Energy Sources (RES)

1. Introduction

Over the past decade, grid-tied PV generation has seen widespread adoption, largely sustained by government subsidies and continuous advancements in power semiconductor technology. Within this domain, primary engineering objectives center on reducing the levelized cost of energy (LCOE) while reinforcing the performance, stability, and conversion efficiency of PV arrays and their associated power converters [1-3]. Growing concerns about climate change and the continuous depletion of fossil fuel resources have accelerated the transition toward renewable energy sources (RES) for sustainable power generation. Among these, PV systems have emerged as a key technology due to their ability to generate clean electricity with minimal environmental impact. Depending on system design and operational requirements, PV installations can operate either in grid-connected mode or as standalone (islanded) systems, offering flexibility for a wide range of applications [4, 5]. A single-stage, three-phase inverter system seems to be the optimal choice for utility-scale high-power PV installations [6]. A comprehensive analysis of the dynamic behavior of photovoltaic distributed generation (PV-DG) systems has become increasingly important, particularly under transient voltage disturbances and varying operating conditions. As the penetration of medium-scale PV installations within distribution networks continues to increase, it is necessary to evaluate their influence on overall network performance and to verify the effectiveness of their control strategies during both steady-state and transient operating conditions. Such an assessment should also consider the interaction of PV-DG systems with existing distribution network equipment, including capacitor banks, voltage regulators, and other voltage control devices, to ensure reliable and stable system operation [7, 8].

The dynamic performance of PV systems is influenced by several factors, including system configuration, control strategies, distribution network characteristics, and environmental conditions. These aspects have been extensively investigated in the existing literature due to their significant impact on system stability and operational performance. Furthermore, numerous studies have proposed a variety of power electronic converter topologies for integrating distributed generation (DG) into electrical distribution networks, each designed to enhance power quality, efficiency, and grid compatibility [9, 10].

Maximum Power Point Tracking (MPPT), a fundamental feature of PV systems for maximizing energy extraction, has been widely investigated in the literature, as reported in [11, 12]. However, the majority of these studies primarily focus on two-stage PV converter configurations. In contrast, comparatively fewer investigations have addressed the stability analysis and independent P and Q control of utility-scale single-stage photovoltaic systems, highlighting the need for further research in this area. Reference [13] presents a high-power, three-phase, single-stage grid-connected (SSGC) PV system that employs a simplified power converter architecture, resulting in improved conversion efficiency compared with conventional two-stage configurations. In addition, transformerless single-stage converter topologies have attracted considerable attention because of their high efficiency, reduced component count, lower cost, and enhanced reliability. However, these advantages are accompanied by new control challenges, particularly in maintaining stable operation, ensuring effective synchronization, and regulating power exchange with the utility grid, as discussed in [14].

Previous research [15] proposed modeling guidelines for the simulation of grid-connected PV systems employing power-signal-based feed forward control within the voltage regulation loop. However, the study primarily focused on system modeling and did not provide a detailed analysis of stability or transient dynamic performance. Reference [16] presents a comprehensive review of the standards, guidelines, and regulatory requirements governing the integration of grid-connected PV systems, covering both national and international interconnection practices. In [17], a simple control strategy for a SSGC PV system was developed to maintain acceptable power quality at the PCC. Furthermore, the increasing deployment of MW-scale PV plants in distribution networks has created a need for detailed investigations into their impact on network operation and controller performance under both steady-state and transient conditions. Such analyses should also account for the interaction of PV systems with distribution network components, including capacitor banks, line-voltage regulators, and other voltage control equipment, as highlighted in [18].

This research proposes the design and implementation of a dq-frame control strategy for a three-phase single-stage grid-connected PV system. The proposed controller is intended to achieve accurate and decoupled regulation of P and Q, thereby improving the dynamic performance of the PV system while enhancing grid support and operational stability. By employing synchronous reference frame (dq-frame) control, the controller generates appropriate current references corresponding to the desired active and reactive power commands and ensures precise current tracking through an inner current control loop. Consequently, the proposed approach enables effective power management and stable grid-connected operation under varying operating conditions [19].

2. System Architecture and Modeling

Figure 1 illustrates the configuration of the single-stage grid-connected PV system considered in this study. The PV array is directly interfaced with the voltage source inverter (VSI) through a DC-link capacitor, which maintains a stable DC bus voltage. The VSI is controlled using a sinusoidal pulse-width modulation (SPWM) technique to produce the required AC output voltage. On the AC side, the inverter is connected to the utility grid through a harmonic filter designed to suppress switching harmonics and improve power quality. The filter consists of a series inductor and a shunt branch comprising delta-connected capacitors with damping resistors connected in series. Furthermore, the proposed system architecture can be readily expanded to higher power ratings by operating multiple PV inverter units in parallel, enabling scalable integration into medium- and large-scale PV installations.

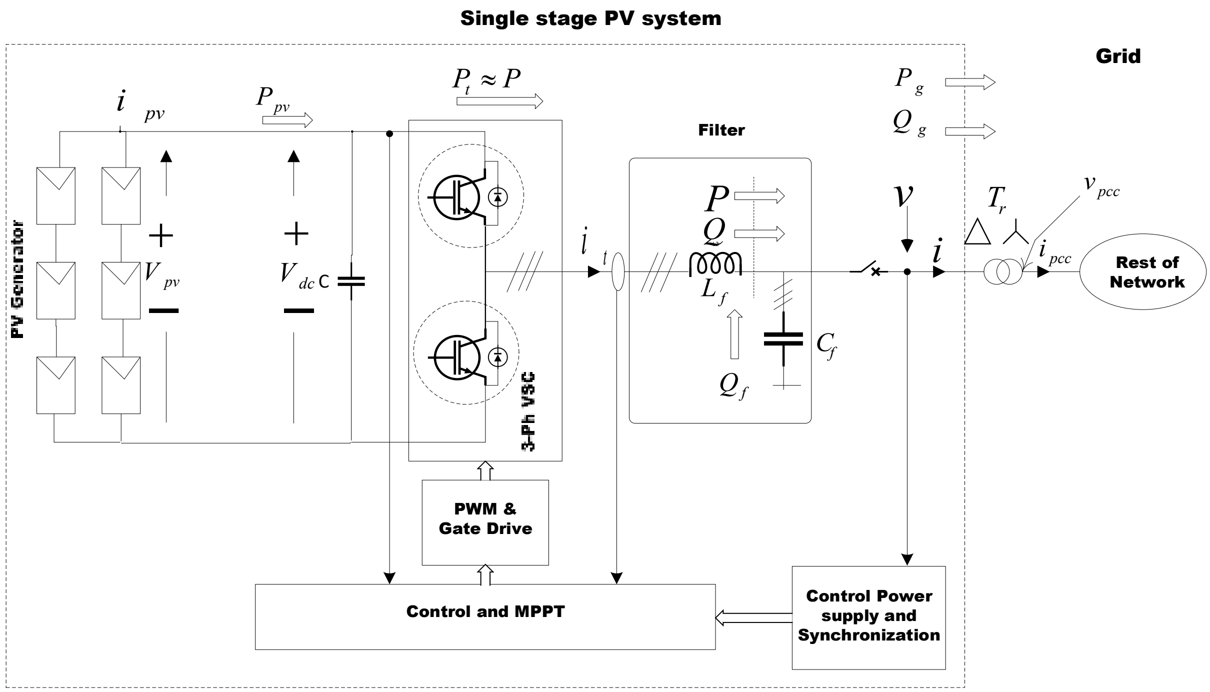

Figure 1. Block Diagram of Grid-Tied Solar PV System

In a grid-connected variable-frequency voltage source converter (VSC) system, applying the αβ reference frame reduces the three-phase variables to two orthogonal components, thereby simplifying the control process compared with the conventional abc reference frame. This transformation enables independent regulation of the active and reactive power exchanged between the VSC and the utility grid. However, the resulting control signals remain sinusoidal and vary with time. As demonstrated in [20], the dq-reference frame preserves the advantages of the αβ transformation while converting the steady-state control variables into constant (DC) quantities. This characteristic simplifies controller design, facilitates compensator implementation, and improves overall control performance, particularly in systems operating under variable-frequency conditions. The PV system illustrated in Figure 1 has been developed to achieve stable and reliable operation while meeting the required performance objectives during normal operation as well as under varying load conditions.

2.1. Grid Synchronization

In the vector diagram shown in Figure 2, an AC voltage vector v rotates in a stationary αβ-frame at an angular frequency ω_0 with an instantaneous angle$\theta(t) = \theta_0 + \omega_0 t$. The SRF-PLL defines a rotating dq-frame at an estimated phase angle$\rho(t) = \rho_0 + \int \omega(\tau)\, d\tau$. Decomposing the voltage vector onto this rotating frame yields a direct-axis component v_d and a quadrature-axis component v_q. When the estimated frame angle ρ aligns perfectly with the actual grid angle θ, the vector lies entirely along the d-axis, driving the quadrature error voltage v_q to zero.

Figure 3 demonstrates how this principle is implemented as a closed-loop control system. The input space vector v undergoes a dq-transformation using the current phase estimate ρ to compute v_d and v_q. The quadrature voltage v_q, serving as the phase error signal, is passed through a loop filter H(s)-typically a PI controller with saturation limits to compute a frequency deviation. This deviation is added to the nominal grid frequency ω_0 to yield the total estimated angular frequency ω. Finally, a Voltage-Controlled Oscillator (VCO), represented by an integrator, integrates ω to continuously update the tracked angle ρ, which is fed back into the dq-transformation block to maintain synchronized phase alignment.

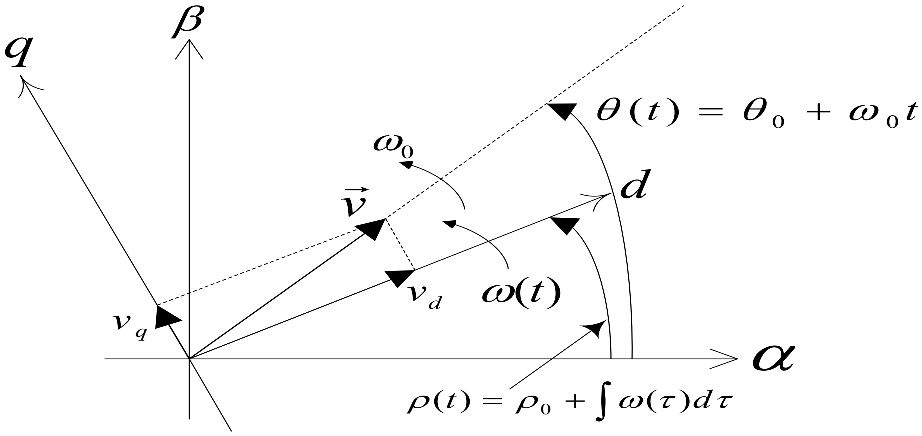

Figure 2. Vector Diagram of PLL

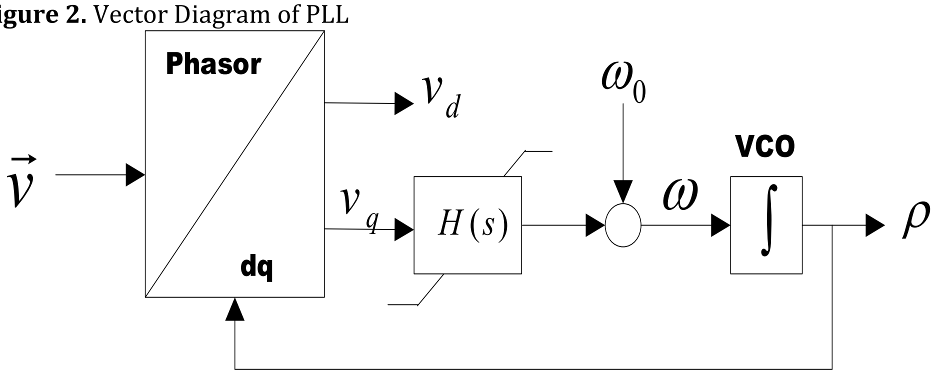

Figure 3. Block diagram of PLL

2.2. Decoupled Active and Reactive Power Control

Block diagram of dq-frame decoupled P and Q control for a grid-connected converter is depicted in Figure 4.

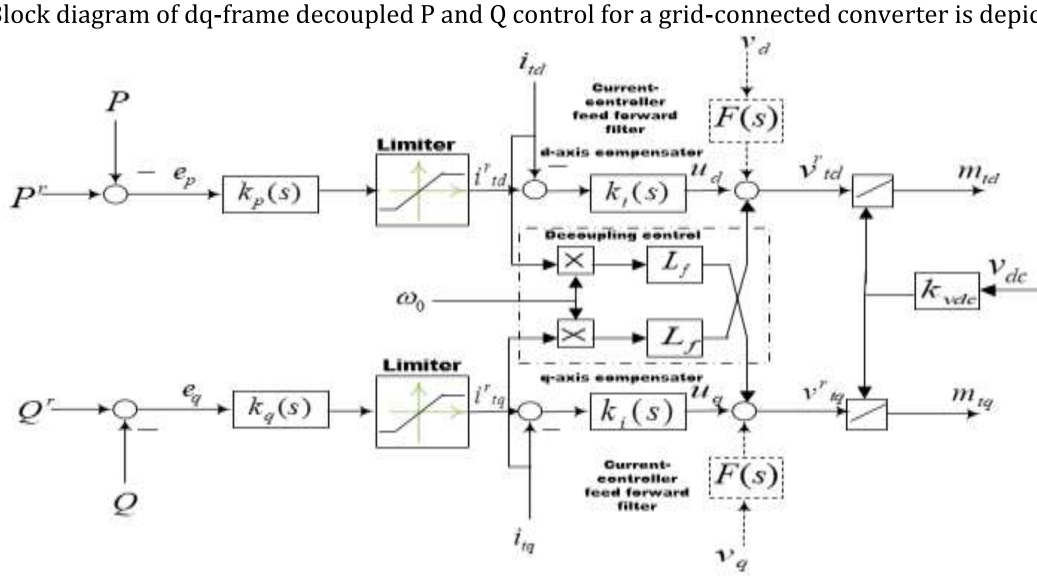

Figure 4. Block Representation of the P and Q Control Strategy Using dq-frame Control

The architecture consists of an outer power control loop and a fast inner current control loop to independently regulate P and Q. In the top channel, the active power error $e_p = P^r - P$ is processed by controller $k_p(s)$ and passed through a limiter to establish the d-axis current reference i_{td}^r. Similarly, in the bottom channel, the

reactive power error $e_q = Q^r - Q$ is passed through controller $k_q(s)$ and a limiter to produce the q-axis current reference i_{tq}^r.
These reference currents are then compared against the measured converter currents (i_{td}, i_{tq}) in the inner control loop, where fast-acting current compensators $k_i(s)$ output intermediate voltage commands u_d and u_q. To ensure independent control of the two axes, a decoupling network cross-feeds the inductive reactance terms $(\omega_0 L_f)$ to cancel out the cross-coupling dynamics caused by the converter's output filter. Additionally, grid voltage components v_d and $v_q$pass through feed forward filters F(s) and are added to the control signals to reject grid disturbances and improve dynamic response. Finally, the resulting terminal reference voltages v_{td}^r and v_{tq}^r are normalized by the measured DC-link voltage v_{dc} to output the dq modulation indices m_{td} and m_{tq}, which drive the PWM switching signals for the converter.
The power P and Q are specified as

$$P_s(t) = \frac{3}{2}[V_{sd}(t) i_d(t)] \tag{1}$$

$$Q_s(t) = -\frac{3}{2}[V_{sd}(t) i_q(t)] \tag{2}$$

As synchronization technique aligns the d-axis voltage vector with the grid voltage vector, resulting in $v_q = 0$, it follows that P and Q are proportional to and may be regulated by

$$i_{dref}(t) = \frac{2}{3V_{sd}} P_{sref}(t) \tag{3}$$

$$i_{qref}(t) = -\frac{2}{3V_{sd}} Q_{sref}(t) \tag{4}$$

This decoupling allows P and Q to be controlled independently using two separate channels, as given in Eq. 3 and Eq. 4 in the outer control loops of the converter architecture.
2.3. Control Architecture for DC-link Voltage Regulation
The closed-loop control architecture for regulating the DC-link voltage V_{dc} in a grid-connected PV inverter system incorporating power feed-forward compensation is depicted in the Figure 5.

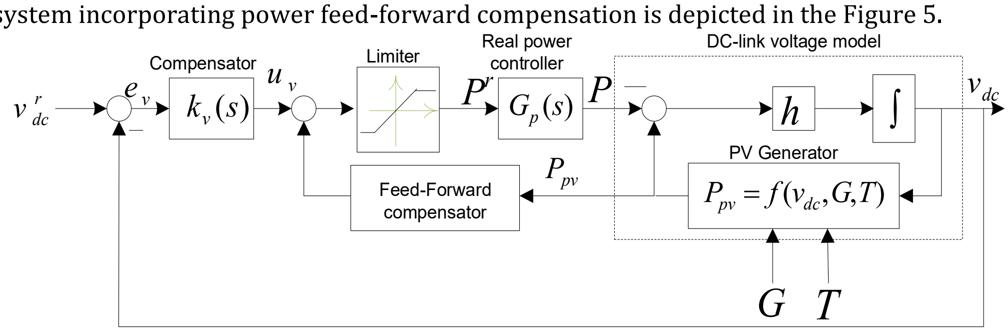

Figure 5. DC-link voltage regulation loop

The control scheme operates by taking the error signal e_v, derived from the difference between the reference voltage v_{dc}^r and the measured DC-link voltage v_{dc}, and processing it through a linear voltage compensator $k_v(s)$ to generate the control effort u_v. To mitigate the impact of sudden environmental variations-such as changes in solar irradiance and ambient temperature-a feed-forward compensator directly incorporates the measured PV power into the loop. This feed-forward path bypasses the outer voltage loop's phase delay, significantly improving transient dynamics during rapid atmospheric transitions. The combined signal passes through a saturation limiter to establish the P^r, which is tracked by the inner real power controller $G_p(s)$ to regulate the grid-injected P. The physical dynamics of the DC link are represented by the power balance node, where the net power mismatch $\Delta P = P_{pv} - p$ charges or discharges the DC-link capacitor.

2.4. Reactive Power and AC Voltage Regulation

The control structure for grid reactive power and AC voltage regulation incorporating filter capacitor feed-forward compensation is illustrated in the Figure 6. The control topology features a dual-mode configuration (Mode A and Mode B) to enable seamless operational flexibility between grid-injected reactive power tracking and PCC AC voltage regulation.

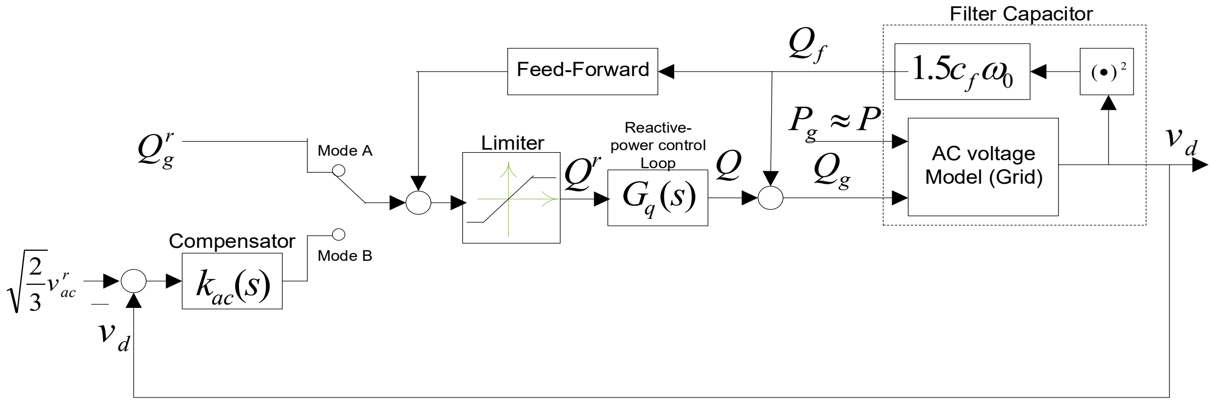

Figure 6. Dual-Mode Control Strategy for Reactive Power and AC Voltage Regulation

In Mode A (Direct Reactive Power Control Mode), the system tracks an external grid reference Q_g^r. In Mode B (AC Voltage Regulation Mode), the measured d-axis grid voltage v_d is subtracted from the scaled reference voltage, and the resulting error signal is processed through an AC voltage compensator $k_{ac}(s)$, to dynamically generate the required reactive power demand.

$$Q_f = 1.5C_f\omega_0\, v_d^2 \quad (5)$$

To account for the reactive power consumed or generated by the AC filter capacitor C_f, a feed-forward path calculates the filter reactive power as given in Eq. 5. The total reactive power delivered to the grid Q_g is formed by the summation of converter power Q and capacitor reactive power Q_f, which directly influences the grid AC voltage model v_d.

3. Results and Discussion

To verify the control strategy, a three-phase SSGC PV system in Figure 1 is simulated in MATLAB/Simulink. The system parameters are listed in Table 1.

Table 1. Simulation Parameters

Symbol	**Description**	**Specifications**
PV Parameters		
P_{max}	PV maximum power	1.5 MW
V_{MPP}	Voltage at Maximum Power	26.3 V
I_{MPP}	Current at Maximum Power	7.61 A
I_{SC}	Short-Circuit Current	8.21 A
V_{OC}	Open-Circuit Voltage	32.9 V
	Number of series-connected Panels	54
	Number of parallel connected Panels	144
Inverter Parameters		
V_{DC}	DC side voltage	1450 V
C	DC Link Capacitor	9625 µf
R	Line Resistance	3.26 mΩ
L	Line Inductance	300 µH
C_f	Filter capacitor	500 µF
f_s	Switching frequency	3.6 kHz

V_s	Grid Voltage	415 V

The system performance is evaluated under different load conditions, with particular emphasis on voltage regulation, power quality, active and reactive power flow, and overall system stability. The test cases considered in this study are given in Table 2.

Table 2. Different test cases for simulation

Number	Load Type	Parameters
Case-1	Linear Balanced RL type load	P = 1 MW, Q= 10kVAr
Case-2	Linear Balanced RL type load	P = 2MW
Case-3	Linear Unbalanced RL type load	Pa=1 MW, Pb=0.9 MW, Pc=0.5 MW, Qa=10 KVAr, Qb= 15 kVAr, Qc=20 kVAr
Case-4	Non Linear Load	3-Ph Bridge Rectifier with RL load (R=0.25Ω and L=10mH)

3.1. Case-1: Performance Evaluation under Linear Balanced RL Type Load

Figure 7 evaluates the dynamic response and steady-state performance of the grid-tied inverter system supplying a linear balanced RL load. A step-change in the load is introduced at t = 0.5 s to examine the controller's transient behavior, power-sharing accuracy, and its ability to maintain power quality at the PCC.

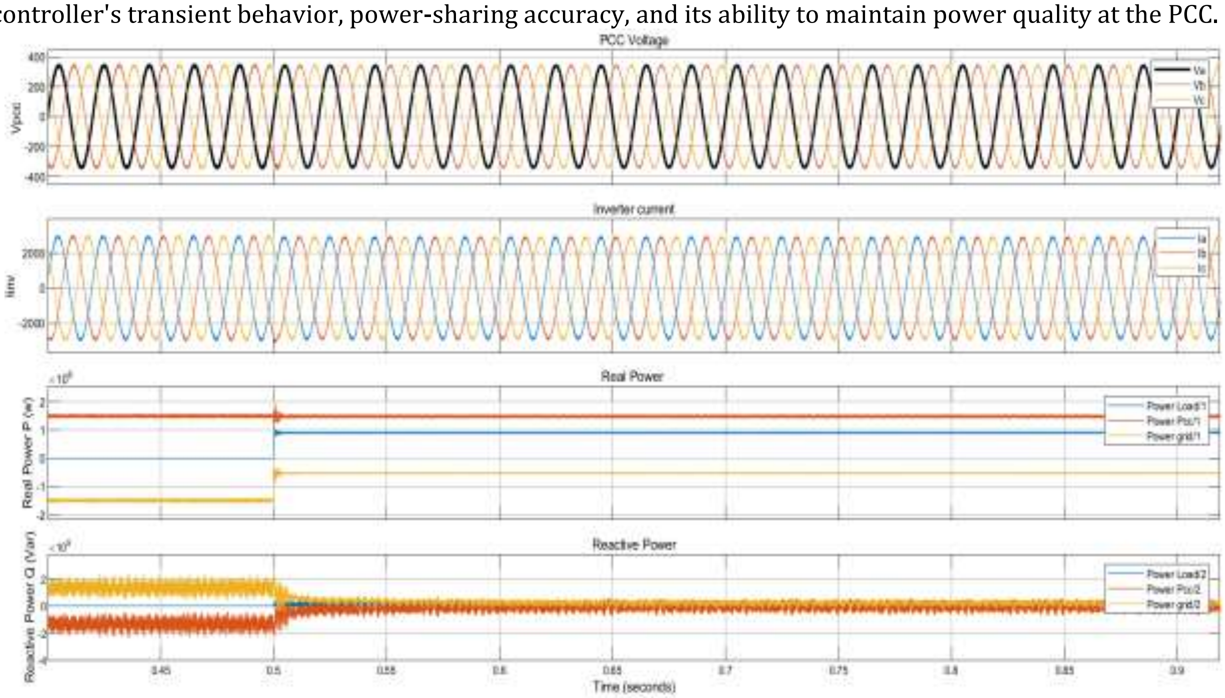

Figure 7. Dynamic response of system under Case 1, Considering Solar Irradiance = 1000 w/m^{2}and Temperature = 25°C.

The voltage waveforms remain strictly sinusoidal, balanced, and constant in amplitude (~ 339 peak) across the entire timeline. Crucially, at the transient switching instant (t = 0.5 s), there is no noticeable voltage sag, swell, or phase distortion. This demonstrates that the grid interface is highly robust and the control system successfully isolates the grid voltage profile from sudden localized load variations.

The load is completely disconnected (P_{Load}=0 W) at t < 0.5 s. The inverter generates a constant active power of P_{pcc}=1.5 MW. Because there is no local load, the entirety of this power is exported to the utility grid, indicated by P_{grid}=-1.5 MW. At t = 0.5 s, the linear balanced RL load is switched on, drawing a step active power of P_{Load}= 1 MW. The inverter output remains undisturbed at 1.5 MW. Consequently, the local load consumes a portion of the inverter's generated power, reducing the surplus power exported to the grid. The grid power shifts smoothly from -1.5 MW to -0.6 MW, satisfying the power conservation law.

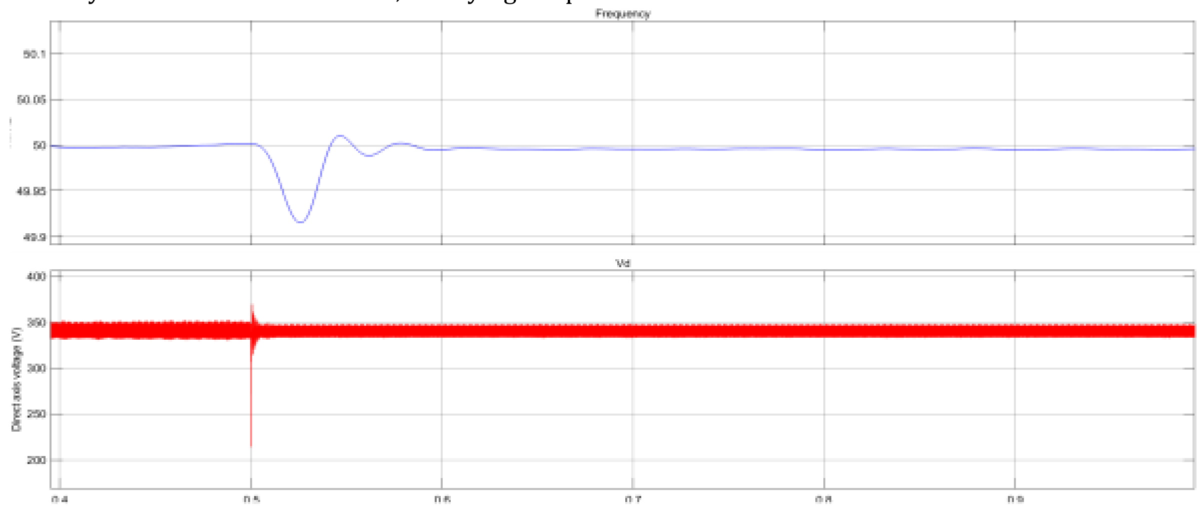

Figure 8. Response of frequency and voltage variation under case-1

Figure 8 evaluates the robustness and dynamic stability of the system's PLL and core voltage controller during the load step-change introduced at t = 0.5 s. The tracking response of the system frequency (f) and the synchronous reference frame direct-axis voltage (V_d) are analyzed to verify grid synchronization integrity. At t < 0.5 s the system operates steadily at its nominal grid frequency of 50 Hz. Upon the introduction of the balanced RL load at t = 0.5 s, a momentary frequency dip occurs due to the sudden active power surge. The frequency drops to a minimum nadir of approximately 49.9 Hz. The frequency control loop, together with the internal PLL, demonstrates a well-damped transient response, restoring the system frequency to its nominal value within approximately 0.1 s. During the disturbance, the peak frequency variation is limited to about +0.085 Hz, corresponding to only 0.17% of the nominal frequency. This indicates effective frequency regulation and demonstrates compliance with the frequency performance requirements specified by IEEE 1547.

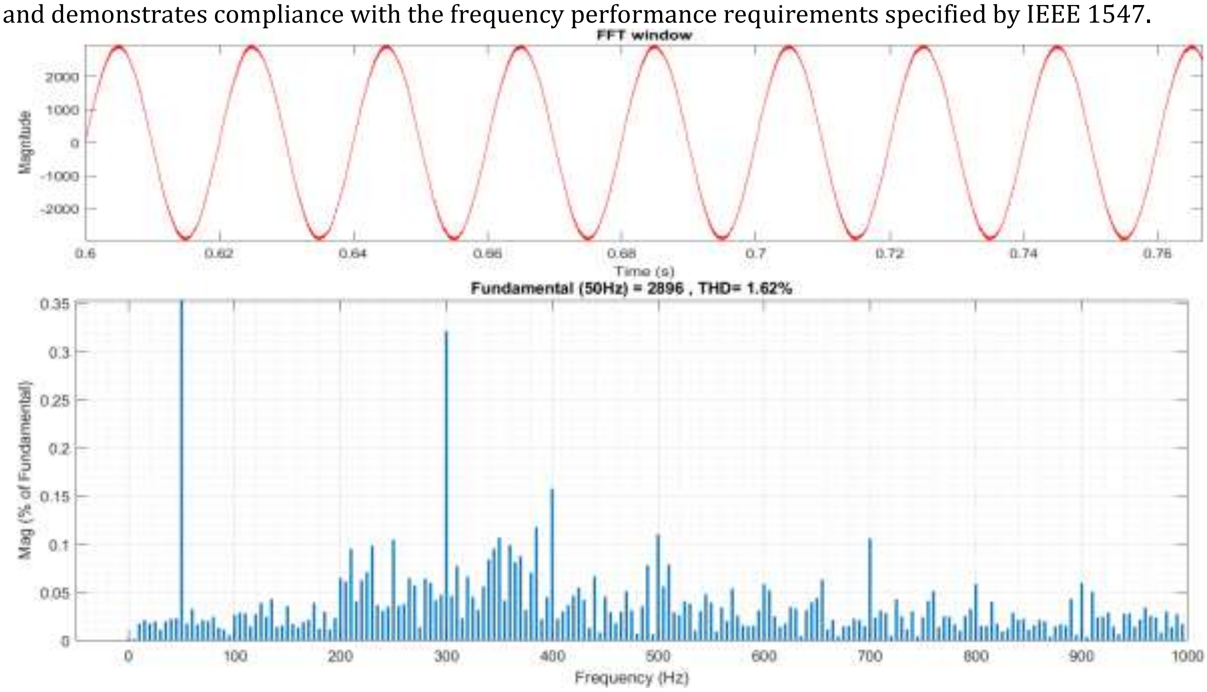

Figure 9. PCC current THD under case 1

The direct-axis voltage component remains well regulated at approximately 340 V under steady-state conditions. When the load step is applied, the voltage experiences a brief transient reduction, reaching nearly

215 V. This short-duration disturbance reflects the rapid action of the current decoupling and voltage control loops in responding to the sudden change in load demand. The voltage subsequently returns to its nominal operating range in less than 0.01 s, with only minor high-frequency oscillations. The fast recovery and limited ripple indicate effective tracking performance and stable operation of the inner control loop.

An FFT-based assessment is performed on the current waveform at the PCC, as presented in Figure 9, to evaluate the power quality performance of the proposed system. The analysis yields a current THD of 1.62%, which is significantly lower than the 5% limit specified by IEEE 519 for the considered grid-interconnection conditions [21]. This low THD value demonstrates the effectiveness of the inverter control strategy in reducing harmonic components and maintaining a nearly sinusoidal current waveform at the PCC.

3.2. Case-2: Performance Evaluation under Linear Balanced RL Type Load exceeding PV capacity

The system's dynamic performance and power-sharing strategy when a heavy load step-change is applied at t = 0.5 s that exceeds the maximum active power generation capability of the PV inverter. This case study verifies the grid's ability to seamlessly transition from an energy-absorbing state to a deficiency-support state while keeping the PCC voltage and inverter current tightly regulated.

At t = 0.5 s, load step-change occurs, demanding P_{load} = 2 MW, exceeds the inverter's maximum output 1.5 MW. To cover the power deficit, the utility grid instantaneously reverses its power flow direction. P_{grid} Transitions from – 1.5 MW to 0.1 MW, feeding power into the local network as shown in Figure 10.

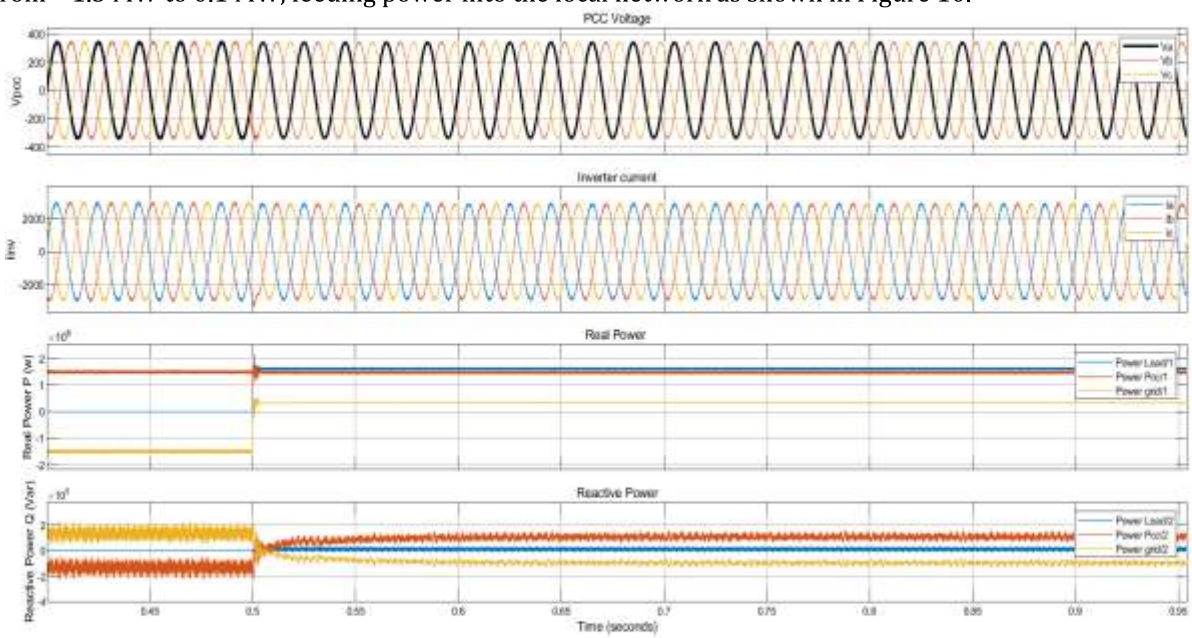

Figure 10. Dynamic response of system under Case 2, Considering Solar Irradiance = 1000 w/$m^2$and Temperature = 25°C.

Under the severe active-power overload condition, the system experiences a pronounced reduction in frequency, with the minimum value reaching approximately 49.85 Hz, as illustrated in Figure 11. Compared with Case 1, the larger frequency excursion is attributed to the greater impact of the sudden power imbalance at the PCC. Despite this disturbance, the frequency returns to its nominal operating range within approximately 0.12 s. The maximum frequency deviation is limited to about 0.15 Hz, corresponding to 0.3%, indicating that the proposed control strategy provides satisfactory frequency regulation and remains within the applicable utility grid-code limits.

At the t = 0.5 s the heavy load is connected, a sharp downward transient spike is observed, dropping momentarily to a minimum of approximately 110 V.

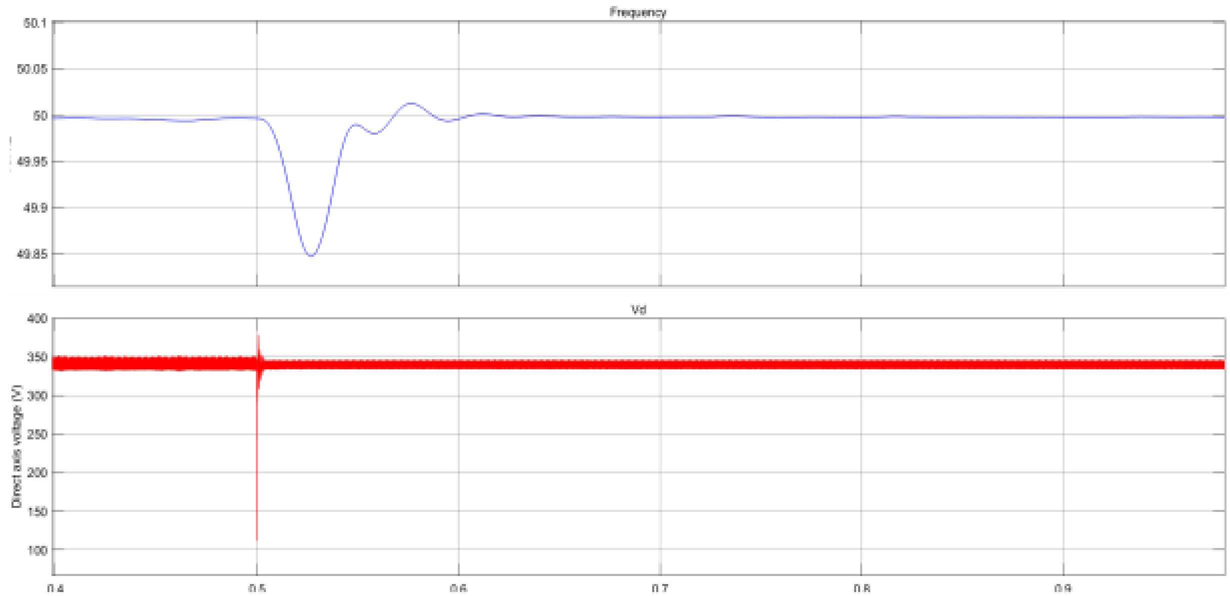

Figure 11. Response of frequency and voltage variation under case-2

3.3 Case-3: Performance Evaluation under Linear Unbalanced RL Type Load

The dynamic and steady-state performance of the grid-tied inverter system under an unbalanced load condition is shown in Figure 12. At t = 0.5 s, an unbalanced three-phase load is connected to the system.

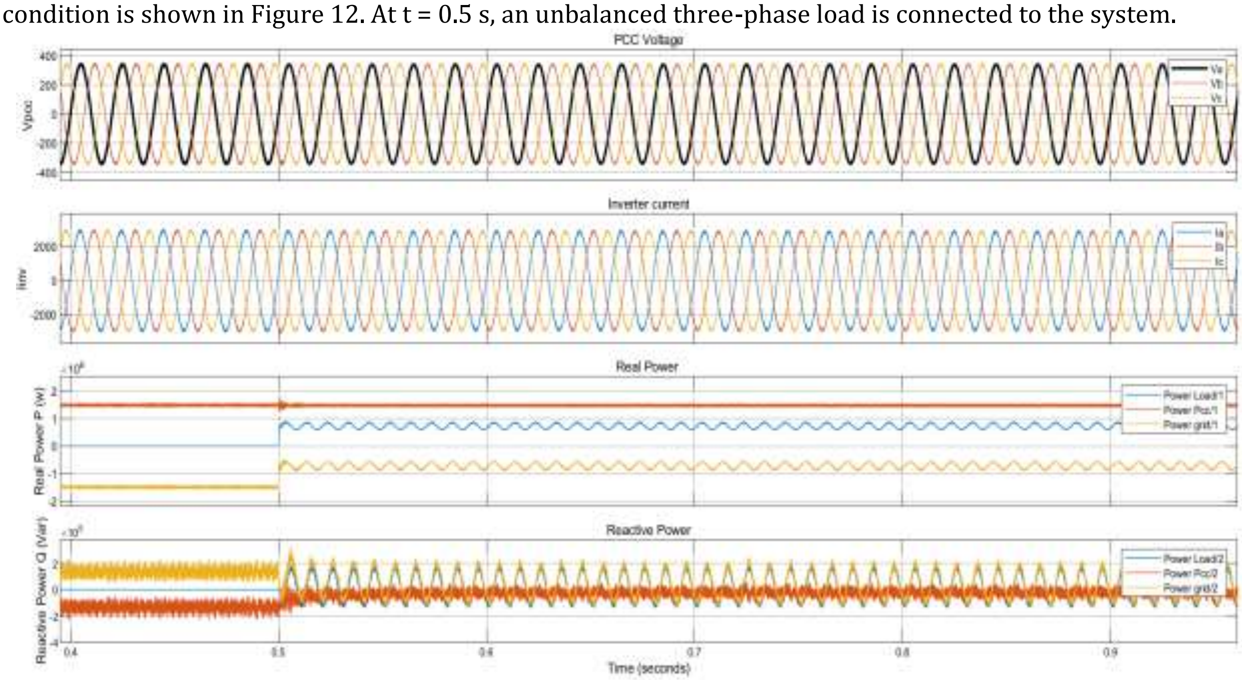

Figure 12. Dynamic response of system under Case 3, Considering Solar Irradiance = 1000 w/m^{2}and Temperature = 25°C.

At t = 0.5 s, the unbalanced load is introduced, drawing an average active power of approximately 0.8 MW. Due to the interaction between positive- and negative-sequence currents and voltages, the load power P_{load} exhibits a significant double grid-frequency oscillation. Because the inverter controller is designed to deliver a strict, ripple-free constant active power P_{pcc} = 1.5 MW, it does not participate in feeding the oscillating power components. Consequently, the utility grid acts as a buffer 100 Hz active power ripple is entirely absorbed by the grid.

At the instant t = 0.5 s the unbalanced load is introduced, a sudden disruption in the instantaneous active power flow causes a localized transient frequency deceleration. The frequency drops to a minimum nadir of approximately 49.93 Hz. V_d exhibits a sharp downward notch, momentary dipping to roughly 280 V as depicted in Figure 13.

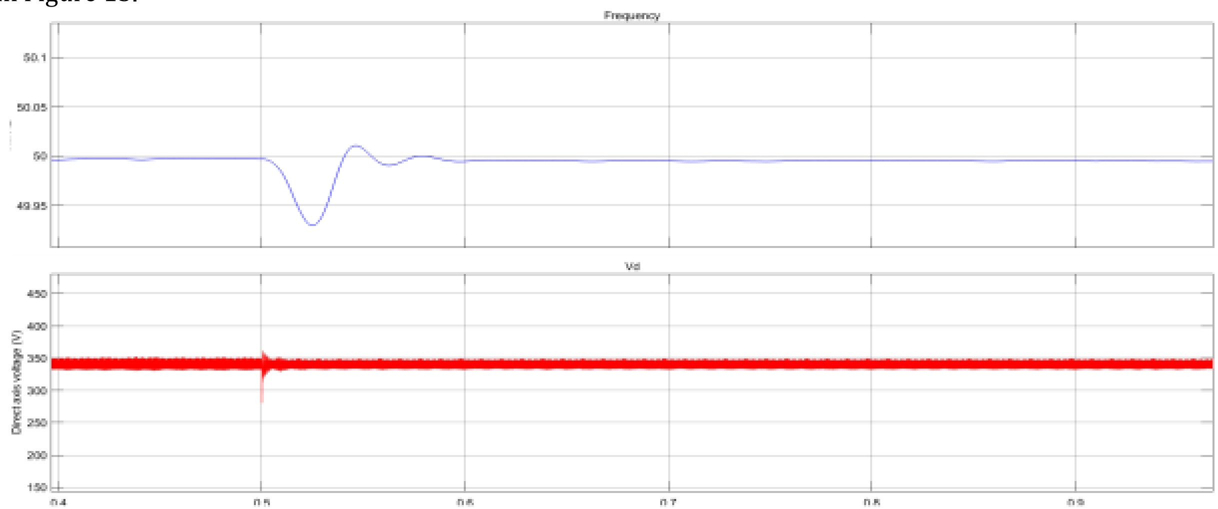

Figure 13. Response of frequency and voltage variation under case-3

The calculated current THD registers at 1.84% as shown in Figure 14. This is exceptionally low and comfortably satisfies the standard 5% maximum limit imposed by the IEEE 519 standard.

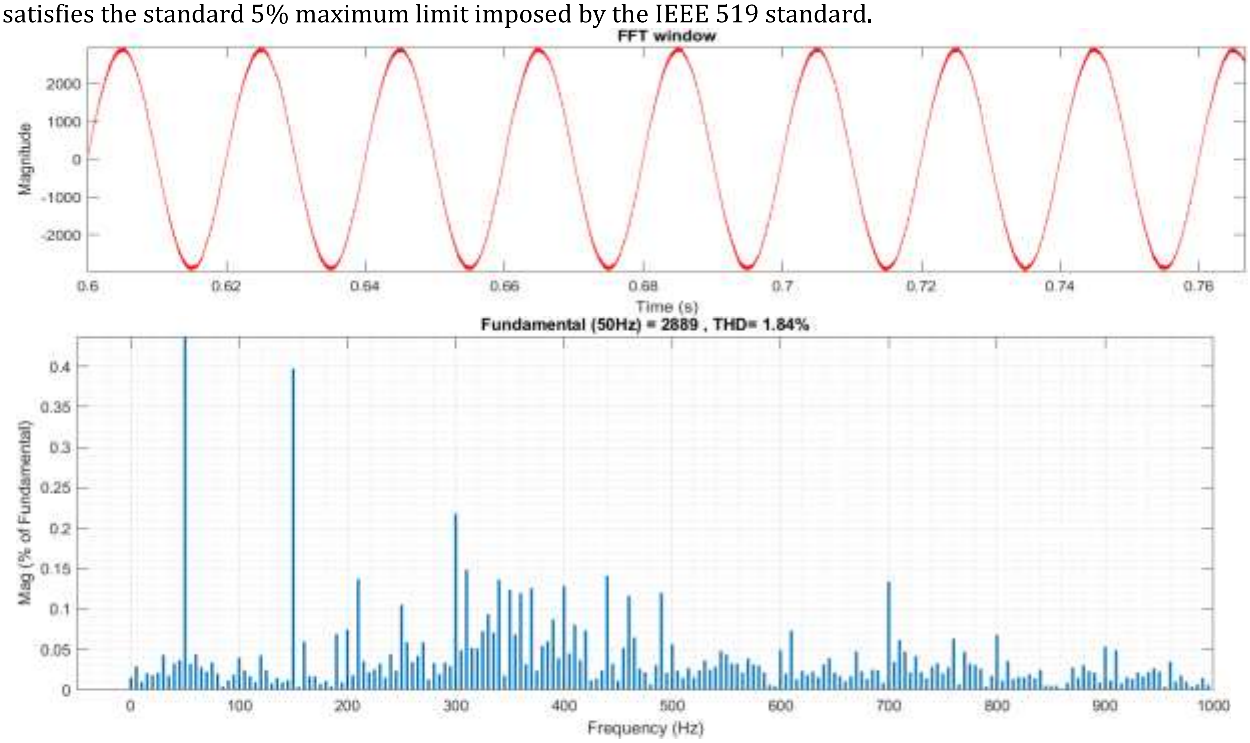

Figure 14. PCC current THD under case 3

3.4 Case-4: Performance Evaluation under nonlinear 3-Ph bridge rectifier with RL Type Load

The system's dynamic and steady-state performance when a 3-Ph non-linear load (such as a diode bridge rectifier feeding a resistive-inductive load) is connected to the network at t = 0.5 s as depicted in Figure 15.

Due to the smoothing characteristics of the load, the active power profile P_{load} exhibits a gradual exponential ramp, eventually settling at a steady-state consumption of approximately 1.1 MW. The inverter output power P_{pcc} stays fixed and perfectly linear at 1.5 MW. Consequently, the grid active power smoothly drops to an average of -0.4 MW continuing to absorb the remaining surplus generation. Because the inverter does not participate in harmonic active power delivery, the high-frequency active power ripples generated by the rectifier stage are seamlessly managed and buffered entirely by the grid.

At t = 0.5 s the non-linear load is introduced, the sudden change in localized current composition causes a transient frequency dip to a nadir of approximately 49.97 Hz as shown in Figure 16. The internal PLL loop filter successfully damps the transient without sustained oscillations, smoothly restoring the frequency back to its nominal value within roughly 0.12 s. Unlike a standard linear load which yields a deep, sharp notch, the non-linear load transition shows an immediate structural widening of the V_d high-frequency ripple band.

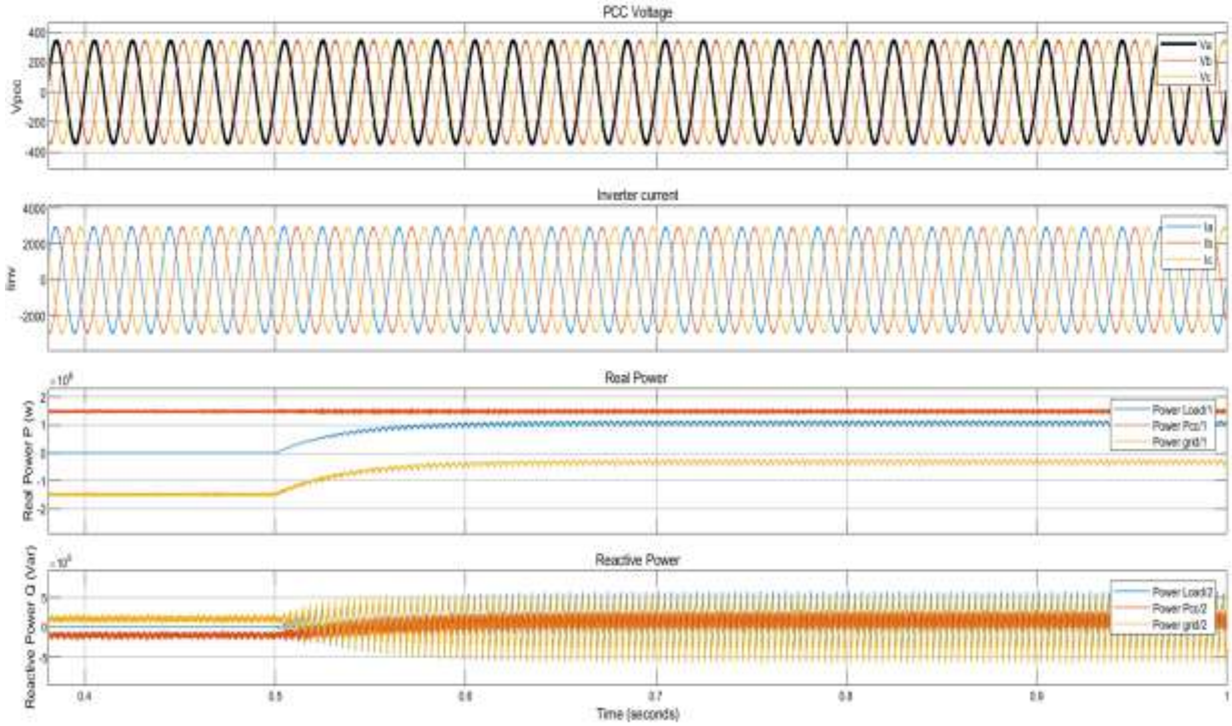

Figure 15. Dynamic response of system under Case 4, Considering Solar Irradiance = 1000 w/m^{2}and Temperature = 25°C.

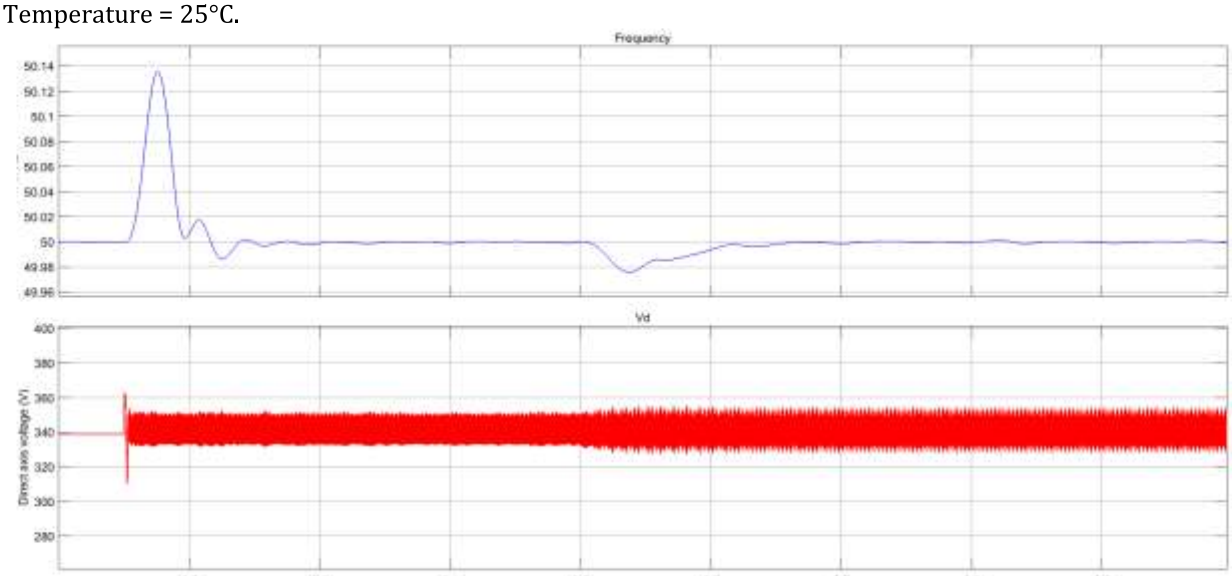

Figure 16. Response of frequency and voltage variation under case-4

The calculated current THD registers at 4.87% as depicted in Figure 17. While this THD value is higher than under normal operating conditions due to the heavy load stress, it remains strictly below the 5% maximum limit mandated by the IEEE 519 standard, certifying acceptable power quality injection even under peak loading conditions.

For both the nominal 1 MW and heavy 1.8 MW balanced linear step-load conditions, the system maintains good power quality, with the current THD remaining at approximately 1.62%. This result indicates effective steady-state current regulation and limited harmonic distortion. When an unbalanced step load is introduced across the three phases, the THD increases marginally to 1.84%. The relatively small change demonstrates the capability of the proposed control architecture to mitigate negative-sequence effects and preserve acceptable power quality under phase-unbalance conditions.

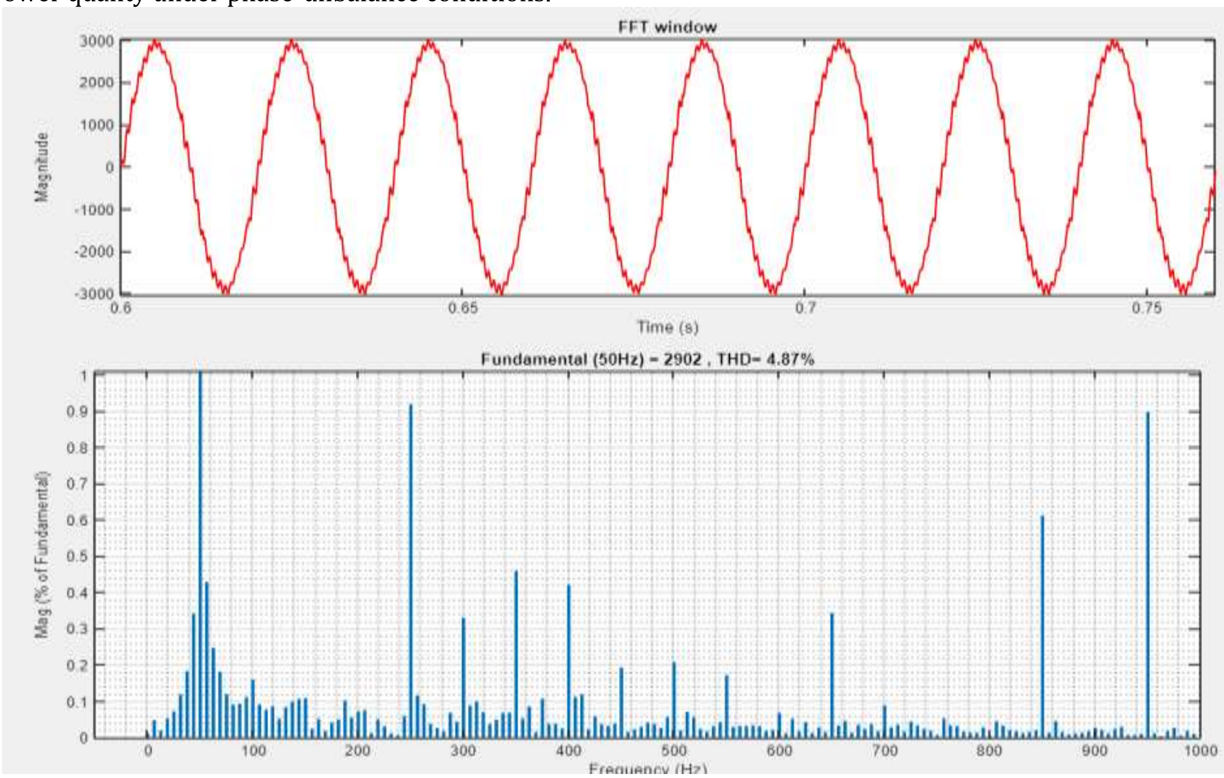

Figure 17. PCC current THD under case 4

Under harmonic-rich stress from a three-phase bridge rectifier, the THD rises to 4.87%. Despite significant non-linear current distortion, the current THD remains below the critical 5% threshold, proving full compliance with the IEEE 519 grid standard.

4. Conclusion

This paper presented an integrated control framework for a grid-connected PV inverter system capable of operating reliably under varying environmental conditions, loading scenarios, and power quality disturbances. The proposed control architecture integrates a SRF-PLL, a decoupled dq-axis current control strategy for independent active and reactive power regulation. The coordinated control structure provides accurate grid synchronization, fast dynamic response, stable DC-link voltage regulation, and effective power quality enhancement at the PCC. Simulation studies carried out under balanced, heavy, unbalanced, and non-linear loading conditions demonstrated the effectiveness of the proposed approach. The controller maintained accurate active and reactive power tracking, minimized DC-link voltage fluctuations during rapid irradiance variations, and achieved low current harmonic distortion while satisfying the IEEE 519 harmonic limits under all operating conditions. Moreover, the proposed dual-mode compensation strategy enabled seamless transition between reactive power control and PCC voltage support, thereby improving voltage stability during grid disturbances. Overall, the proposed control strategy offers a reliable and practical solution for enhancing the dynamic performance, power quality, and grid support capability of SSGC PV systems. The results indicate that the proposed framework is well suited for future power systems with high PV penetration, where reliable grid support and compliance with grid codes are essential.

References

1. Karuppiah N, Mounica P, Bhanutej JN, Saravanan S, Reddy R, Israni R. Revolutionizing Renewable Energy Integration: The Innovative Gravity Energy Storage Solution. E3S Web Conf. 2024;547. DOI: 10.1051/e3sconf/202454703028
2. Jain S, Agarwal V. A Single-Stage Grid Connected Inverter Topology for Solar PV Systems With Maximum Power Point Tracking. IEEE Trans Power Electron. 2007;22(5):1928–40. DOI: 10.1109/TPEL.2007.904202
3. Petrone G, Spagnuolo G, Teodorescu R, Veerachary M, Vitelli M. Reliability Issues in Photovoltaic Power Processing Systems. IEEE Trans Ind Electron. 2008;55(7):2569–80. DOI: 10.1109/TIE.2008.924016
4. Aisyah Mohd Yusof N, Ali Z. Review of Active Synchronization for Renewable Powered Microgrid. Int J Eng Technol [Internet]. 2019 Jan 18;8(1.7 SE-Articles):14–21. Available from: https://doi.org/10.14419/ijet.v8i1.7.25950 DOI: 10.14419/ijet.v8i1.7.25950
5. Murillo-Yarce D, Alarcón-Alarcón J, Rivera M, Restrepo C, Muñoz J, Baier C, et al. A Review of Control Techniques in Photovoltaic Systems. Sustainability [Internet]. 2020;12(24). Available from: https://www.mdpi.com/2071-1050/12/24/10598 DOI: 10.3390/su122410598
6. Zhu Y, Yao J, Wu D. Comparative study of two stages and single stage topologies for grid-tie photovoltaic generation by PSCAD/EMTDC. In: 2011 International Conference on Advanced Power System Automation and Protection. 2011. p. 1304–9. DOI: 10.1109/APAP.2011.6180580
7. Katiraei F, Agüero JR. Solar PV Integration Challenges. IEEE Power Energy Mag. 2011;9(3):62–71. DOI: 10.1109/MPE.2011.940579
8. Israni RK, Yadav R, Singh R, Reddy BR. Power Quality Enhancement in Wind-Hydro Based Hybrid Renewable Energy System by Interlocking of UPQC. In: 2023 3rd International Conference on Energy, Power and Electrical Engineering (EPEE). 2023. p. 112–23. DOI: 10.1109/EPEE59859.2023.10352036
9. Ko SH, Lee SR, Dehbonei H, Nayar C V. Application of voltage- and current-controlled voltage source inverters for distributed generation systems. IEEE Trans Energy Convers. 2006;21(3):782–92. DOI: 10.1109/TEC.2006.877371
10. Carrasco JM, Franquelo LG, Bialasiewicz JT, Galvan E, PortilloGuisado RC, Prats MAM, et al. Power-Electronic Systems for the Grid Integration of Renewable Energy Sources: A Survey. IEEE Trans Ind Electron. 2006;53(4):1002–16. DOI: 10.1109/TEC.2006.877371
11. Esram T, Chapman PL. Comparison of Photovoltaic Array Maximum Power Point Tracking Techniques. IEEE Trans Energy Convers. 2007;22(2):439–49. DOI: 10.1109/TEC.2006.874230
12. Jain S, Agarwal V. Comparison of the performance of maximum power point tracking schemes applied to single-stage grid-connected photovoltaic systems. IET Electr Power Appl. 2007;1(5):753–62.
13. Lal VN, Siddhardha M, Singh SN. Control of a large scale single-stage grid-connected PV system utilizing MPPT and reactive power capability. IEEE Power Energy Soc Gen Meet. 2013;1–5.
14. Mastromauro RA, Liserre M, Dell'Aquila A. Control issues in single-stage photovoltaic systems: MPPT, current and voltage control. IEEE Trans Ind Informatics. 2012;8(2):241–54.
15. Yazdani A, Di Fazio AR, Ghoddami H, Russo M, Kazerani M, Jatskevich J, et al. Modeling Guidelines and a Benchmark for Power System Simulation Studies of Three-Phase Single-Stage Photovoltaic Systems. IEEE Trans Power Deliv. 2011;26(2):1247–64.
16. Wu YK, Lin JH, Lin HJ. Standards and Guidelines for Grid-Connected Photovoltaic Generation Systems: A Review and Comparison. IEEE Trans Ind Appl. 2017;53(4):3205–16.
17. Purohit PJ, Jadeja MG, Jotangiya VG, Chauhan PH, Vaghela DJ. Improvement of Power Quality in Single Stage Grid Connected PV System with Novel Configuration of Multilevel Inverter. SSRG Int J Electr Electron Eng. 2024;11(4):234–9.
18. Sonawane AJ, Umarikar AC. Voltage and Reactive Power Regulation With Synchronverter-Based Control of PV-STATCOM. IEEE Access. 2023;11:52129–40.
19. IEEE Application Guide for IEEE Std 1547TM-2018, IEEE Standard for Interconnection and Interoperability of Distributed Energy Resources with Associated Electric Power Systems Interfaces. IEEE Std 15472-2023 (Revision IEEE Std 15472-2008). 2024;1–291.
20. A. Yazdani RI. Voltage-Sourced Converters: Modeling, Control, and Applications. Hoboken, New Jersey: John Wiley & Sons, Inc.; 2010.
21. IEEE Standard for Harmonic Control in Electric Power Systems. IEEE Std 519-2022 (Revision IEEE Std 519-2014). 2022 Aug;1–31.